ADVANCED HEALTHCARE MATERIALS
www.advhealthmat.de
www.MaterialsViews.com

Enzyme-Responsive Cell-Penetrating Peptide Conjugated Mesoporous Silica Quantum Dot Nanocarriers for Controlled Release of Nucleus-Targeted Drug Molecules and Real-Time Intracellular Fluorescence Imaging of Tumor Cells

Jinming Li, Fang Liu, Qing Shao, Yuanzeng Min, Marianne Costa, Edwin K. L. Yeow, and Bengang Xing**

Here, a set of novel and personalized nanocarriers are presented for controlled nucleus-targeted antitumor drug delivery and real-time imaging of intracellular drug molecule trafficking by integrating an enzyme activatable cell penetrating peptide (CPP) with mesoporous silica coated quantum dots nanoparticles. Upon loading of antitumor drug, doxorubicin (DOX) and further exposure to proteases in tumor cell environment, the enzymatic cleavage of peptide sequence activates oligocationic TAT residues on the QDs@mSiO2 surface and direct the DOX delivery into cellular nucleus. The systematic cell imaging and cytotoxicity studies confirm that the enzyme responsive DOX-loaded CPP-QDs@mSiO2 nanoparticles can selectively release DOX in the tumor cells with high cathepsin B enzyme expression and greatly facilitate DOX accumulation in targeted nucleus, thus exhibiting enhanced antitumor activity in these cells. As contrast, there is limited nuclear-targeted drug accumulation and lower tumor cytotoxicity observed in the cells without enzyme expression. More importantly, significant antitumor DOX accumulation and higher tumor inactivation is also found in the drug resistant tumor cells with targeted enzyme expression. Such simple and specific enzyme responsive mesoporous silica-QDs nanoconjugates provide great promise for rational design of targeted drug delivery into biological system, and may thus greatly facilitate the medical theranostics in the near future.

1. Introduction

Cancer is one of the major causes of death in the world to date, and incidences of cancer continue to increase at an alarming rate.[1] Currently, chemotherapy is still the major treatment of choice in most cases, however, the systemic toxicity, the lack of tumor specificity, and the emergence of multidrug resistance (MDR) remain the serious problems, which limit the extensive applications of targeted chemotherapy in clinical practice.[2] The rational design to enhance the capability of therapeutic reagents to reach their designated cellular targets will therefore be of clinical importance to meet up the challenging requirements for improved therapeutic efficacy and minimum side effects. Recent advances in multifunctional nanomedicine have shown great potentials to address such challenges by integration of antitumor reagents or other biologically active molecules with various types of biocompatible nanomaterials as intracellular transport cargo systems to efficiently target the desired cellular structures to achieve early diagnosis of diseases, noninvasive imaging, and efficient tumor therapy with reduced toxicity.[3] However, most of the current investigations mainly concerned the intracellular delivery of nanomaterials into the cytoplasm through the well-known endocytosic uptake pathways, and the loaded therapeutic agents or diagnostic moieties were normally released into cytosol instead of cell nucleus,[4] where the genetic process and the transcription machinery locate, and more importantly, they are usually direct targets recognized by numerous antitumor therapeutic agents including doxorubicin (DOX) and cisplatin and so on to terminate tumor cell growth. Therefore, the rational design of simple and effective strategies that enable nuclear-targeted therapy by delivering anticancer therapeutic agents directly into tumor cell nucleus to sustain potent therapeutic effects will be highly expected in clinics.

Recently, some cell-penetrating peptides (CPPs) represented by TAT, polyarginine, transportan, and penetratin, and so on[5] have been widely proposed as powerful transport vector tools to conjugate with different types of functional nanomaterials including metallic nanoparticles,[6] quantum dot clusters (QDs),[7] mesoporous silica ($mSiO_2$) nanoparticles,[8] upconversion nanoprobes,[9] magnetic nanoparticles,[10] functionalized micelles and

Dr. J. Li, F. Liu, Q. Shao. Dr. Y. Min, M. Costa, Prof. E. K. L. Yeow, Prof. B. Xing
Division of Chemistry and Biological Chemistry
School of Physical and Mathematical Sciences
Nanyang Technological University,
Singapore 637371, Singapore
E-mail: edwinyeow@ntu.edu.sg; Bengang@ntu.edu.sg

DOI: 10.1002/adhm.201300613

liposomes,[11] to mediate intracellular nucleus-targeted delivery of therapeutic agents or imaging contrast molecules in different type cells mostly by taking advantage of the strong electrostatic interactions between these cationic CPP-modified nanotransporters and the negatively charged cell membrane components. Despite of their considerable clinical potentials in principle, the majority of established CPP-modified delivery nanoplatforms lack cell or tissue specificity;[5] the CPP nanoconjugates and their attached therapeutic molecules or imaging probes can be dispersed in any cell in contact throughout the living systems and cannot effectively accumulate in the target tumor sites only, thus obviously compromising the therapeutic efficacy, especially for those drug molecules working toward cell nucleus as their final targeting destination. The absence of tumor cell specificity and potential risk of drug-induced toxicity to healthy tissues has therefore urgently initiated extensive research efforts to develop smart and personalized activatable delivery cargo systems capable of responding to tumor microenvironment and selectively endowing CPP-modified nanoconjugates with targetable capability for specific targeting drug delivery.

Currently, a variety of CPP-modified nanomaterials with their sensitive responses to cell environmental perturbations including pH, temperature, and redox reactions[12] have been introduced as smart nanocarriers to selectively activate CPPs at the target tumor sites to control the localized delivery of therapeutic reagents or genes into the molecular targets within the cells for the purpose of enhanced antitumor treatment and minimized side effects. Several enzyme-sensitive nanomaterials have also been successfully designed to react with specific intracellular proteases including matrix metalloproteinases (MMPs) and so on to improve the retention of the imaging contrast agents, chemotherapeutic drug molecules, plasmid DNA or small interfering RNAs into the targeted tumor cells for noninvasive trafficking of operative process and significant increasing of chemotherapeutic efficacy in vitro and in vivo;[13] however, the systematic investigations toward the development of multifunctional activatable CPP functionalized antitumor drug nanoconjugates that can sensitively respond to the specific enzymes in the microenvironment of tumor cells to enable the effective nuclear-targeted tumor treatment by selectively triggering the localized activation of CPP nanocarriers, and simultaneously to achieve real-time monitoring of therapeutic dynamics remains a critical challenge in the field and there is still an urgent need to further explore this pertinent study.

Here, we present a rational design of a set of multifunctional antitumor drug nanocarriers by introduction of an enzyme activatable CPP sequence onto mesoporous silica-coated QDs surface, which allows the nuclear-targeted delivery and controlled release of the encapsulated DOX into the nucleoplasm of tumor cells, and simultaneously enables the observation of the nuclear internalization in real-time mostly by taking advantages of the unique fluorescent properties of semiconductor QDs nanocrystals including tunable emission spectra, enhanced brightness, superior photostability, and simultaneous excitation of multiplexing fluorescence colors.[14] Upon surface coating with mesoporous silica and further covalently conjugating with an activatable CPP sequence containing a nuclear-targeted oligocationic TAT peptide, a short enzyme-cleavable peptide linker and an anionic-inhibitory domain sequence to neutralize the positive charges in the whole peptide structure, the activatable CPP mesoporous silica-coated QDs (CPP-QDs@$mSiO_2$) nanocarriers could sensitively respond to specific tumor protease cathepsin B, one type of frequently encountered cleavable enzyme that is closely associated with tumor diseases.[15] Generally, the CPP-QDs@$mSiO_2$ nanocarriers were stable and inactive in the cells without cathepsin B expression, however, after the internalization into the targeted tumor cells with this enzyme, the specific enzymatic cleavage of peptide linker in the whole peptide sequence would selectively remove the anionic sequence from CPP-QDs@$mSiO_2$ surface and the exposed CPPs would directly drive the delivery of CPP-modified nanoparticles and loaded antitumor DOX drug into cell nucleus, thus realizing the improved nucleus-targeted chemotherapy in both drug sensitive and resistant tumor cells. Importantly, apart from the nuclear-oriented antitumor drug delivery, this CPP-QDs@$mSiO_2$ nanoconjugate also demonstrated the promising function to real-time monitor the cellular trafficking of released DOX molecules under living conditions, which therefore provides a great possibility for selective nucleus target-controlled release and real-time imaging in tumor therapy.

2. Results and Discussion

2.1. Synthesis and Characterization of Enzyme Responsive CPP-QDs@$mSiO_2$

As a proof of concept, **Scheme 1** illustrated the rational design of the enzyme-responsive CPP-QDs@$mSiO_2$ nanocarriers to selectively control the nuclear-targeted antitumor drug delivery and real-time image of the intracellular trafficking of released drug molecules in living cells. Typically, the synthesis of surface-functionalized QDs@SiO_2 was carried out on the basis of the method reported previously.[16] Upon the surface etching with NaOH solution, the core–shell mesoporous silica-coated QDs nanocrystals would be produced (QDs@$mSiO_2$),[17] which exhibited the advantages to stabilize nanoparticle suspensions in biological environment and to facilitate easy surface modification for further biomedical applications.

In order to achieve enzyme-responsive nuclear-targeted antitumor drug release, an activatable CPP sequence was first prepared by solid-phase peptide syntheses, which consists of three units including a cysteine-containing cationic TAT peptide (CRRRQRRKKR) for nucleus targeting, an enzyme-responsive linker PGFK to sensitively respond to cathepsin B protease, and an oligoanionic-inhibitory domain (EEEEEE) to greatly neutralize the charge distribution of the whole peptide sequence. Then, the prepared activatable CPP sequence was conjugated with amino-functionalized mesoporous QDs@$mSiO_2$ nanoparticles, which were first modified with *N*-hydroxysuccinimide (NHS)-containing oligo(ethylene) glycol maleimide (NHS-dPEG_2-maleimide) linker to afford the maleimide-dPEG_2 QDs@$mSiO_2$ structures. Upon the specific reaction between maleimide and thiol groups in the peptide sequence, the enzyme-responsive CPP-QDs@$mSiO_2$ nanoconjugates were finally generated. The diameter and size distribution of the CPP-QDs@$mSiO_2$ nanocarriers were investigated by scanning electron microscopy (SEM) and transmission electron

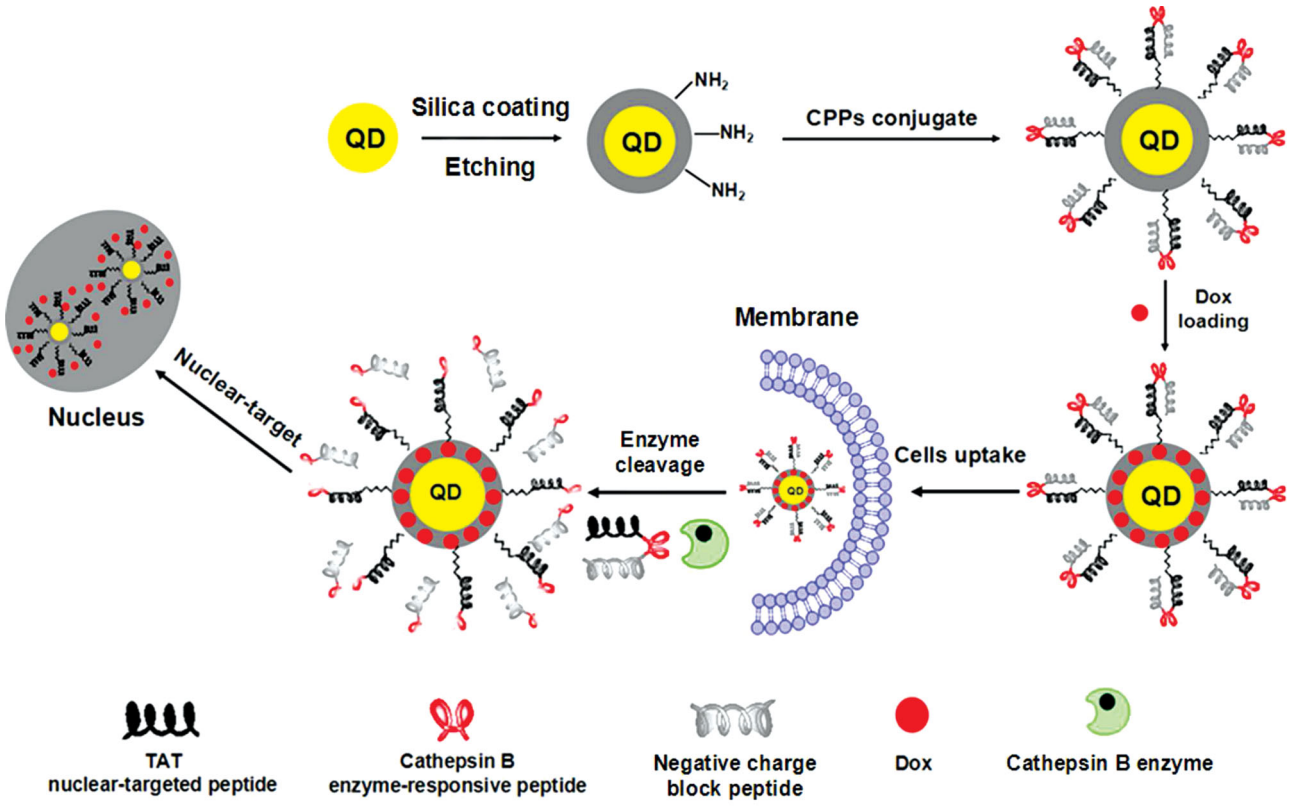

Scheme 1. Schematic illustration of the enzyme-responsive nuclear-targeted CPP-QDs@mSiO$_2$ nanoparticles for selective control of nucleus-targeted drug release and real-time intracellular fluorescence imaging of tumor cells.

microscopy (TEM) (**Figure 1**). The results indicated the narrow size distribution of the nanoparticles with an overall diameter of 40 nm, which would be the suitable size to achieve effective cell penetration and targeted nuclear delivery.[18] Importantly, the absorption and fluorescent studies indicated that the TGA-QDs and the core–shell mesoporous QDs@mSiO$_2$ exhibited similar luminescent properties that will be useful for in vitro and living cell imaging studies (Figure S1, Supporting Information).

2.2. Live Cell CLSM Imaging of CPP-QDs@mSiO$_2$ for Enzyme-Responsive Nuclear Targeting

We further determined the feasibility of the enzyme-responsive nuclear-targeted CPP-QDs@mSiO$_2$ nanoconjugate to mediate the transport into the cell nucleus under living cell environment with cathepsin B expression using confocal laser scanning microscopy (CLSM). In this study, the tumor cell line

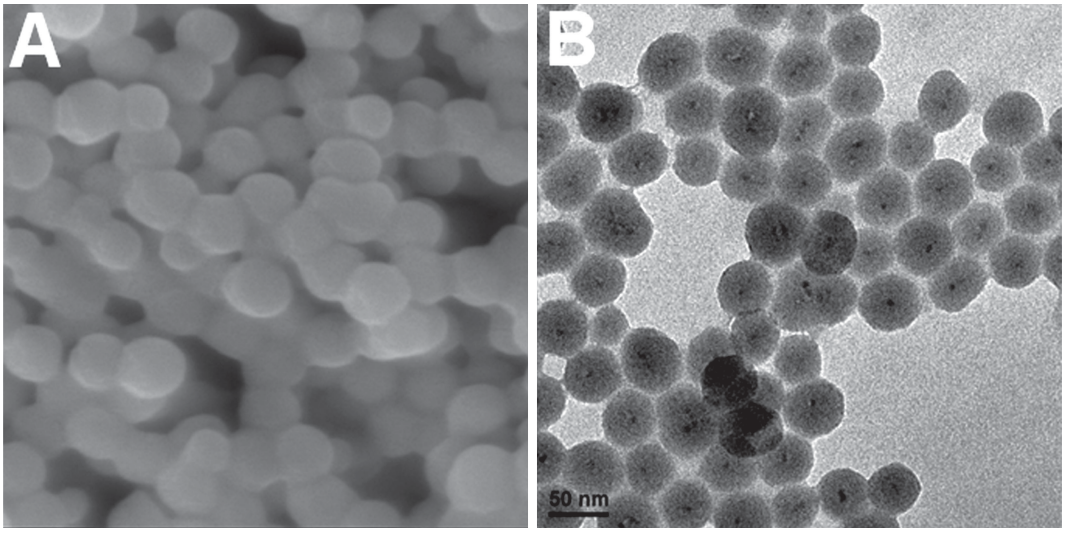

Figure 1. The size distributions of enzyme-responsive nuclear-targeted CPP-QDs@mSiO$_2$ nanoparticles, determined by A) SEM and B) TEM.

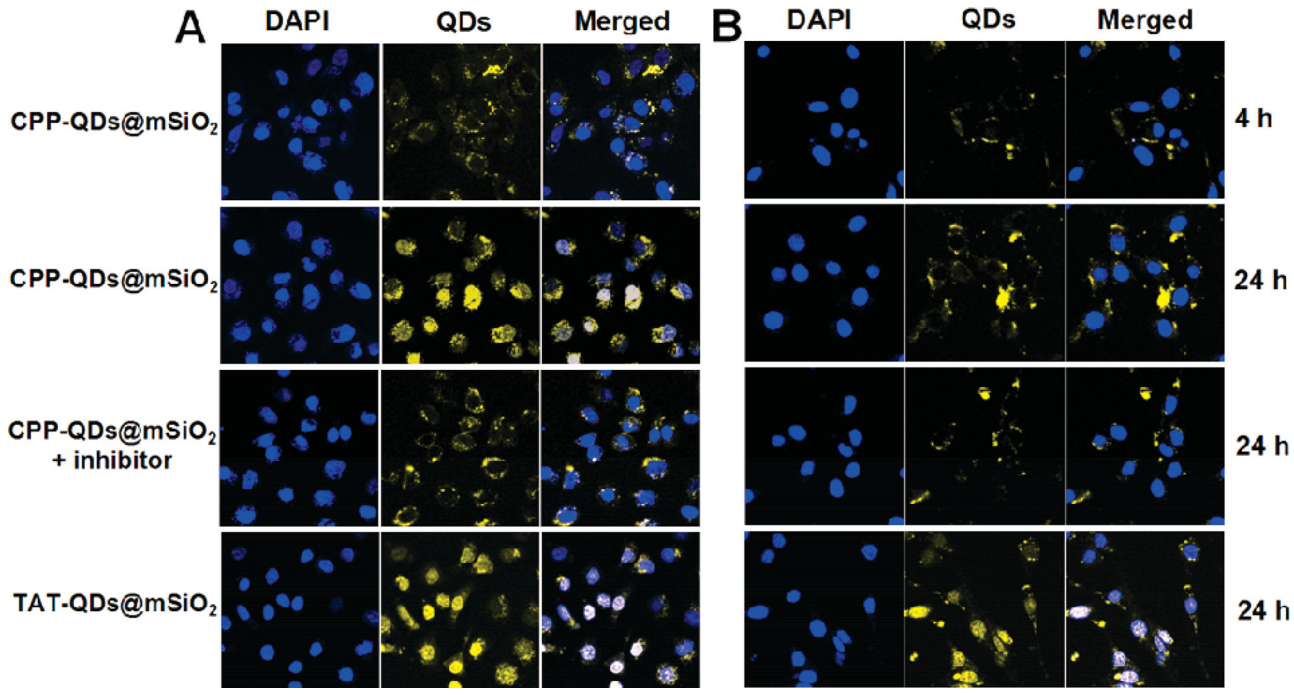

Figure 2. Live cells image of the enzyme-responsive nuclear-targeted CPP-QDs@$mSiO_2$ nanoparticles in A) cathepsin B-positive cells A549 and B) cathepsin B-negative cells NIH-3T3. The cathepsin B inhibitor, antipain hydrochloride (5×10^{-6} M), was used to block enzyme activity. The concentration of the CPP-QDs@$mSiO_2$ nanoparticles was 50 μg mL^{-1}. The filter sets for CPP-QDs@$mSiO_2$ Ex: 405 nm, Em: 550/30 nm.

A549 with highly expressed protease cathepsin B was chosen as a target. As a negative control, NIH-3T3 cells were used as there was no cathepsin B expression in the cells. Both A549 and NIH-3T3 cells were cultured and incubated with 50 μg mL^{-1} of enzyme-responsive CPP-QDs@$mSiO_2$ nanoconjugates in Dulbecco's Modified Eagle Medium (DMEM) at 37 °C for different time durations to obtain effective live cell imaging. The cellular uptake and intracellular trafficking were investigated by monitoring of the fluorescence of silica-coated QDs. As shown in **Figure 2**, after 4 h of incubation, there was weak yellow fluorescence observed in A549 cells (Figure 2A), which was mostly in the cytoplasm as confirmed by co-staining of DAPI molecules in cell nucleus, indicating that CPP-QDs@$mSiO_2$ conjugates could be internalized by A549 cells through the established endocytosic pathway (Figure S2, Supporting Information). Under prolonged cellular incubation (24 h), the QDs fluorescent signals become stronger and most of the signals were observed mainly in the nucleus rather than in the cytoplasm of A549 cells. In addition, the similar cellular incubation with treatment of antipain hydrochloride, an efficient cathepsin B enzyme inhibitor[19] was also conducted in A549 cells and the fluorescent signals were mainly accumulated in the cytoplasm and not in the nuclei as observed for similar A549 cell incubation but without inhibitor pretreatment. As contrast, there was yellow fluorescence detected when the enzyme-responsive CPP-QDs@$mSiO_2$ nanoconjugates were incubated with NIH-3T3 and the more significant fluorescent signals were obtained under the conditions of longer time incubation (Figure 2B). Unlike the fluorescence in cell nuclei as observed in A549 cells, most of the yellow fluorescence in controlled NIH-3T3 cells was found mainly in the cytoplasm. Moreover, the controlled cellular imaging by using cationic TAT peptide-modified QDs@$mSiO_2$ clearly indicated that both A549 and NIH-3T3 cells could uptake this positively charged nanoparticle conjugate and the fluorescence was mostly observed in the cell nucleus, suggesting that TAT peptide could efficiently direct nucleus targeting in both A549 and NIH-3T3 cells, which was in good accordance with most of the results reported previously.[8a] These cellular imaging results confirmed that the enzyme-responsive CPP-QDs@$mSiO_2$ nanoconjugates could easily enter into the intracellular cytoplasm. Only upon the interaction of nanoconjugates with specific cathepsin B enzyme in targeted cell line microenvironment would the oligoanionic inhibitory sequence (EEEEEE) dissociate from CPP-QDs@$mSiO_2$ nanoconjugates surface and the activated TAT peptide QDs@$mSiO_2$ could then easily drive the QDs@$mSiO_2$ nanoparticles internalization into cell nucleus. More importantly, the standard 3-(4,5-dimethylthiazol-2-yl)-2,5-diphenyltetrazolium bromide (MTT) assay demonstrated the minimum cytotoxicity of CPP-QDs@$mSiO_2$ nanoconjugates to various types of cell lines (Figure S3, Supporting Information), making the enzyme-responsive CPP-QDs@$mSiO_2$ attractive as an effective transporter cargo for subsequent nucleus-targeted antitumor drug delivery and intracellular tumor imaging in real-time.

2.3. Controlled Release of DOX from Enzyme-Responsive CPP-QDs@$mSiO_2$ Nanocarriers in Buffer Solutions and in Live Cells

We next studied the loading of antitumor drug into enzyme activatable CPP-QDs@$mSiO_2$ nanocarriers and further examined

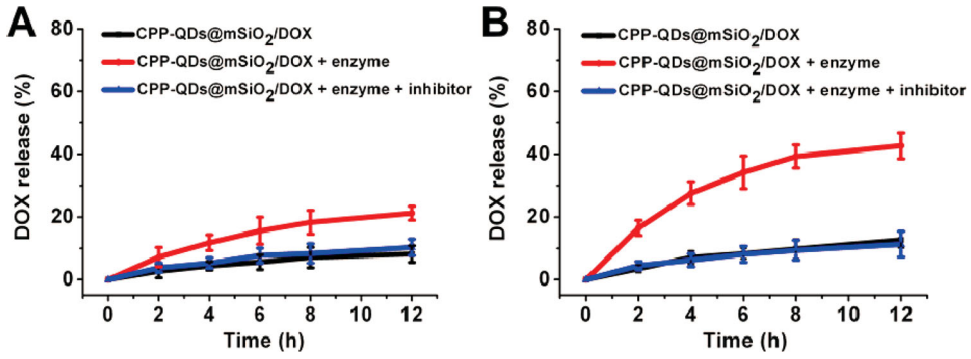

Figure 3. DOX release efficiency from DOX-loaded nanoparticles upon enzyme treatment at different pH in PBS. A) pH 7.4, B) pH 5.5. The concentration of cathepsin B was 50×10^{-9} M and the concentration of cathepsin B inhibitor was 50×10^{-6} M.

their ability to selectively target cell nucleus upon specific enzyme cleavage. Typically, the mesoporous CPP-QDs@$mSiO_2$ nanocarriers were soaked in a DMSO solution containing lipophilic antitumor DOX drug for 12 h. Upon removal of unbound DOX molecules through centrifugation and repeated washing with phosphate-buffered saline (PBS, pH 7.2, 10×10^{-3} M), the successful loading of DOX into mesoporous CPP-QDs@$mSiO_2$ structure was confirmed by the difference in UV–vis absorbance of DOX (Figure S4, Supporting Information), from which optimal drug loading was determined to be 10.7%, comparable to most of the DOX nanoparticle conjugating systems reported previously.[20] After effective loading of DOX into the CPP-QDs@$mSiO_2$, the enzyme-responsive controlled release of DOX from drug-loaded CPP-QDs@$mSiO_2$ nanoparticles was investigated by analysis of fluorescence of DOX in the presence or absence of cathepsin B enzyme under different pH conditions (7.4 and 5.5). As showed in **Figure 3**, there was limited DOX release from drug-loaded CPP-QDs@$mSiO_2$ nanoparticles in the absence of cathepsin B enzyme at pH of 5.5 and 7.4. In the presence of cathepsin B enzyme, the obvious DOX release from the nanoparticles surface could be observed under prolonged enzyme treatment. There was more significant DOX release detected under pH of 5.5 than that of neutral pH conditions, which was mostly attributed to the higher activity of cathepsin B enzyme under acidic environment.[15] As a control, in the presence of enzyme pretreated with antipain hydrochloride, there was less DOX release under both acidic and neutral pH conditions, clearly indicating that the drug-loaded CPP-QDs@$mSiO_2$ nanoconjugates could respond to specific enzyme under acidic conditions and thus lead to the effective drug release from the surface of nanoparticles.

Furthermore, we also performed cellular imaging studies to evaluate the feasibility of controlled DOX release and targeted nuclear delivery on the basis of the enzyme-responsive DOX-loaded CPP-QDs@$mSiO_2$ nanoparticles. In this study, A549 and NIH-3T3 cells were first chosen to incubate with drug-loaded CPP-QDs@$mSiO_2$ nanoparticles. As contrast, similar imaging measurements were also conducted by incubating the cell lines with free DOX. The cellular imaging was monitored by the fluorescence of DOX and QDs, respectively. As shown in **Figure 4**, after 4 h of incubation, both yellow and red fluorescent colors under individual emission filter sets were observed in A549 and NIH-3T3 cells and the fluorescent signals were mainly found in the cytoplasm instead of in the cell nuclei.

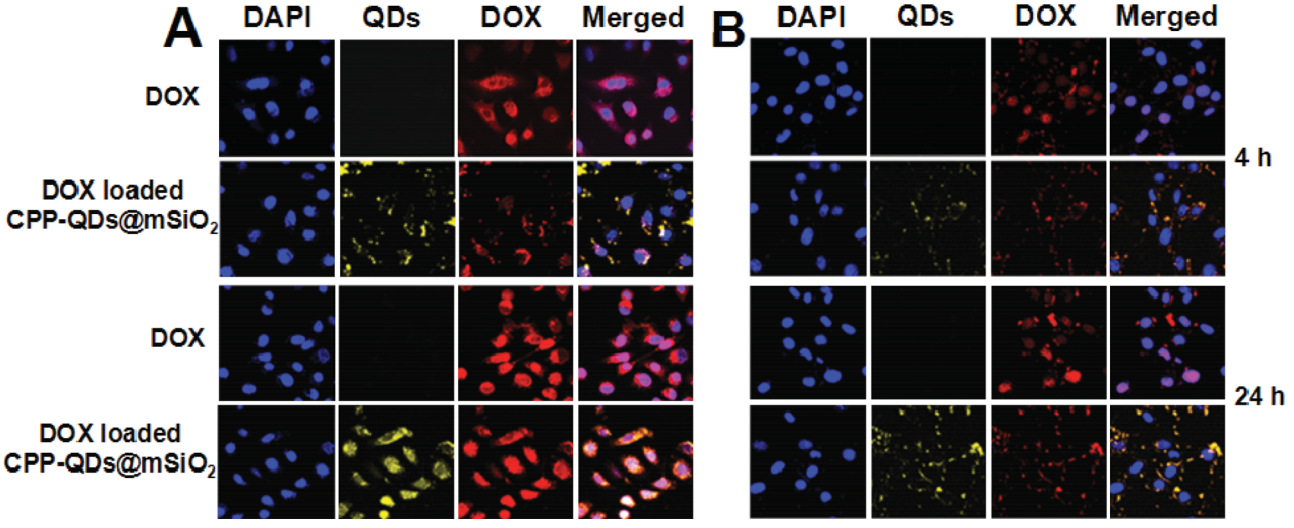

Figure 4. Live cells image of DOX release from drug-loaded CPP-QDs@$mSiO_2$ nanoparticles (DOX: 5 μg mL^{-1}) in A) A549 cells and B) NIH-3T3 cells for 4 h and 24 h incubation. The free DOX (5 μg mL^{-1}) was used as control. The imaging filter sets for CPP-QDs@$mSiO_2$ nanoparticles Ex: 405 nm, Em: 550/30 nm; and for DOX Ex: 488 nm, Em: 630/20 nm.

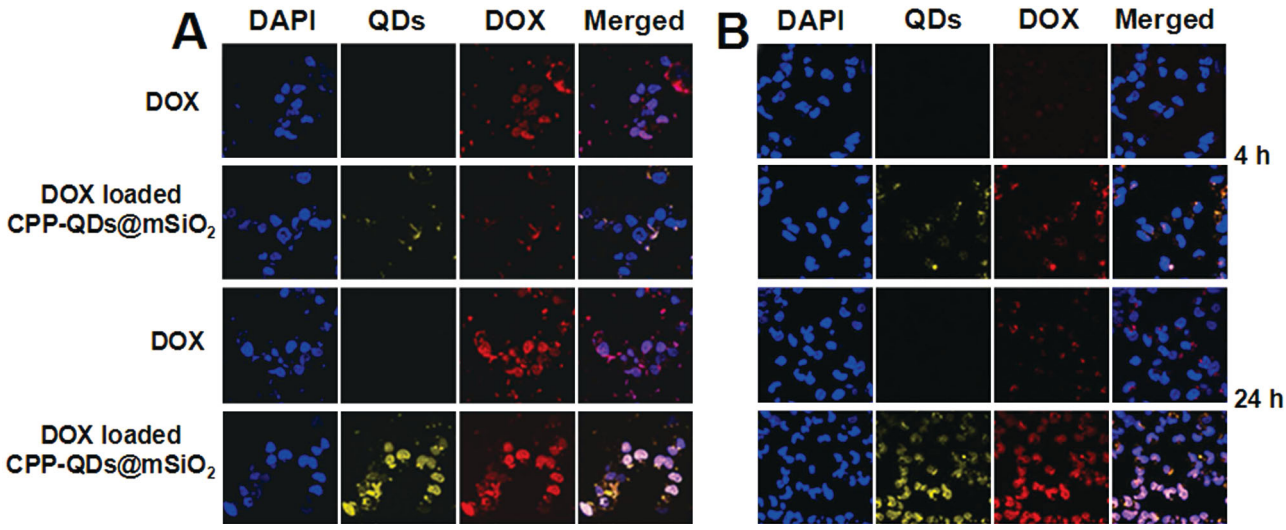

Figure 5. Live cells image of DOX release from drug-loaded CPP-QDs@$mSiO_2$ nanoparticles (DOX: 5 μg mL^{-1}) in nonresistant tumor cells and drug-resistant cells under 4 h and 24 h incubation. A) A2780, B) A2780/Adr. The free DOX (5 μg mL^{-1}) was used as control. The imaging filter sets for CPP-QDs@$mSiO_2$ nanoparticles Ex: 405 nm, Em: 550/30 nm; and for DOX Ex: 488 nm, Em: 630/20 nm.

After longer time incubation to 24 h, more significant yellow and red fluorescence could be detected in A549 and NIH-3T3 cells. In comparison, most of the yellow and red fluorescent signals were mainly accumulated in cell nucleus of A549 cells (Figure 4A), whereas in NIH-3T3 cells, the yellow and red fluorescence were mostly located in the cytoplasm instead of the cell nucleus (Figure 4B). The different location of fluorescent signals observed in these two cells demonstrated that the enzyme-responsive DOX-loaded CPP-QDs@$mSiO_2$ nanoparticles could be internalized into both A549 and NIH-3T3 cells, and more importantly, unlike the case in NIH-3T3 cells, after endocytotic uptake of DOX CPP-QDs@$mSiO_2$, the drug-loaded nanoparticle conjugate would sensitively respond to the specific cathepsin B enzyme in A549 cell environment and the efficient enzyme cleavage could remove the negatively charged oligoanionic inhibitory sequence (EEEEEE) from the activatable CPP sequence. The activated cationic TAT peptide-modified QDs@$mSiO_2$ would thus enable nucleus-targeted DOX delivery into A549 cells. Controlled cell imaging experiments by using free DOX indicated obvious fluorescence in the nucleus of A549 and NIH-3T3 cells and the stronger red fluorescence signals in both nuclei were also observed upon longer time cell incubation, indicating different cell internalization between free DOX drug molecules and enzyme activatable CPP-QDs@$mSiO_2$. The passive diffusion of free DOX into cells would result in rapid accumulation of drug into cell nucleus and therefore induce DNA damage and cytotoxicity in the cells.[21]

More importantly, similar cell imaging measurements were also performed to examine the possibility whether the enzyme-responsive nuclear-targeted DOX-loaded nanoparticles could be used to overcome drug resistance in targeted tumor cells. Typically, two tumor cells including one nonresistant A2780 cells and one DOX-resistant ovarian A2780/Adr cells were used as our main targets to incubate with DOX-loaded CPP-QDs@$mSiO_2$ nanoparticles at 37 °C under different time intervals. As negative controls, these two cells were also incubated with free DOX. As shown in **Figure 5**, after short time (e.g., 4 h) incubation, the yellow and red fluorescence could be detected in the cytoplasm in both A2780 and A2780/Adr cells upon co-staining with DAPI. Longer time incubation (e.g., 24 h) of DOX-loaded CPP-QDs@$mSiO_2$ nanoparticles would lead to more significant fluorescence and the fluorescence was obviously found in the nucleus of A2780 and A2780/Adr cells, suggesting the involvement of endocytosis to uptake the drug-loaded CPP-QDs@$mSiO_2$ nanoparticles into tumor cells at initial stage, and after intracellular internalization, the specific cathepsin B in both drug susceptible and resistant tumor cell structures would efficiently cleave CPP sequence on nanoparticle surface, which locally activated TAT-modified QDs@$mSiO_2$ and thus achieve targeted DOX drug delivery into the nucleus of A2780 and A2780/Adr cells. As contrast, control experiments by incubation of free DOX with A2780 cells even within short-time duration would lead to bright red fluorescence in the cell nucleus and relatively weak fluorescence in the cytoplasm, clearly displaying different uptake pathways when compared with DOX-loaded QDs@$mSiO_2$ nanoparticles. Unlike the effective cellular uptake in A2780 cells, similar imaging analysis by incubation of DOX with resistant A2780/Adr cells showed the significant weak red fluorescence in this cell, indicating the limited free DOX drug uptake in A2780/Adr cells, most likely attributed to the principal multidrug resistant mechanisms that actively expelled chemotherapeutic drugs from the targeted tumor cell structures.[2] These live cell imaging studies clearly suggested that the developed enzyme-responsive DOX-loaded CPP-QDs@$mSiO_2$ nanoconjugate may serve as effective transporter cargoes to selectively direct the delivery of antitumor drugs into cell nucleus upon the activation by specific protease enzyme in the targeted tumor cell environment, and more significantly, the higher cellular internalization of antitumor drugs could probably contribute to circumventing the resistant effect and therefore greatly improve chemotherapy efficacy.

2.4. Nucleus-Targeted Cell Viability via the Enzyme-Responsive CPP-QDs@mSiO$_2$ Nanoparticles

Encouraged by the favorable imaging studies in living cells, we finally evaluated in vitro antitumor activity of the prepared enzyme-responsive DOX-loaded CPP-QDs@mSiO$_2$ nanoparticles and free DOX in the different cell lines (e.g., A549, NIH-3T3, and A2780) including those with antitumor drug resistance (e.g., A2780/Adr). The cell viability was measured by standard MTT assay. In this typical study, the different cell lines were used to incubate with DOX-loaded CPP-QDs@mSiO$_2$ nanoparticles and free DOX, respectively. As shown in **Figure 6**, incubation of different concentrations of free DOX with cathepsin B expressed A549 and A2780 cells for 24 h would result in effective cytotoxicity. For example, the obvious cell viability to A549 and A2780 cells was found to be 75% and 77%, respectively, when 10 μg mL^{-1} of DOX was applied. The more significant cytotoxicity to these cells was further found (e.g., the cell viability dropping to 65% for A549 and 68% for A2780) when higher concentrations of DOX were used (e.g., 20 μg mL^{-1}), suggesting the rapid diffusion of free DOX into nonresistant cell structures to sustain the effective cytotoxicity. However, unlike the potent activity observed in cathepsin B expressed A549 and A2780 cells, free DOX displayed limited drug activity (85% cell viability) to the drug resistant A2780/Adr cells even under conditions with higher concentration (e.g., 20 μg mL^{-1}), mostly owing to the limited drug accumulation caused by the multidrug resistant mechanisms in A2780/Adr cells. Compared with free DOX drug molecules, incubation of different concentrations of enzyme-responsive drug-loaded CPP-QDs@mSiO$_2$ with A549, A2780, and A2780/Adr cells was also performed to evaluate the potential antitumor activity. As indicated in Figure 6, under similar effective DOX concentration, drug-loaded CPP-QDs@mSiO$_2$ exhibited higher antitumor activity, especially for the cells (A2780/Adr) with potent drug resistance when compared with cells treated with free DOX only. For example, upon incubation of 10 μg mL^{-1} of enzyme-responsive DOX-loaded CPP-QDs@mSiO$_2$, the cell viability to A549, A2780, and A2780/Adr cells was determined to be 68%, 67%, and 71%, respectively, which was lower than the values observed in the cells treated with free DOX only. In addition, more significant activities could be observed when higher concentration of drug-loaded CPP-QDs@mSiO$_2$ (e.g., 20 μg mL^{-1}) and longer incubation time were applied (Figure 6 and Figure S5, Supporting Information). However, similar cell incubation of enzyme-responsive drug-loaded CPP-QDs@mSiO$_2$ with A549, A2780, and A2780/Adr cells, which have been pretreated with antipain hydrochlorite cathepsin B inhibitor (5×10^{-6} M), would lead to significantly limited cytotoxicity in these three cells as compared with the drug activities observed in studies in the absence of inhibitor, indicating that cathepsin B inhibitor could easily block the potent antitumor cytotoxicity to the enzyme expressed tumor cells along the incubation of drug-loaded CPP-QDs@mSiO$_2$. Furthermore, the cell viability analysis by incubation of free DOX and drug-loaded CPP-QDs@mSiO$_2$ with controlled NIH-3T3 cells without

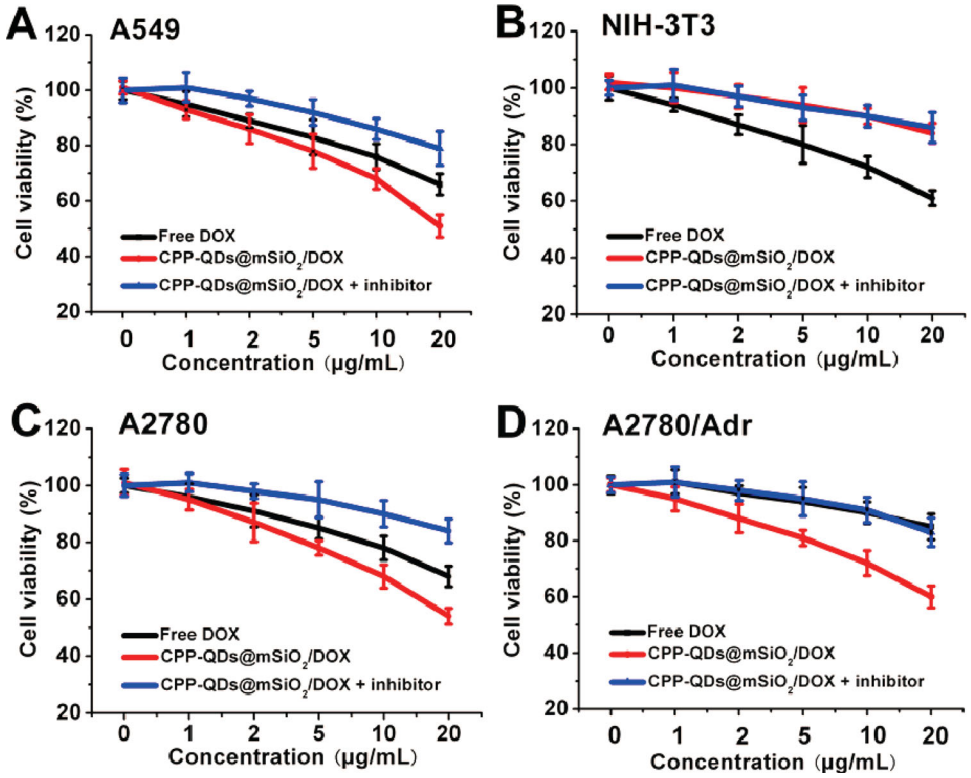

Figure 6. The cell viability of enzyme-responsive DOX-loaded CPP-QDs@mSiO$_2$ nanoparticles at different concentrations of DOX in A) A549 cells; B) NIH-3T3 cells; C) A2780 cells and D) A2780/Adr cells. The cathepsin B inhibitor, antipain hydrochloride (5×10^{-6} M), was used to block enzyme activity. Free DOX was used as contrast. The incubation time: 24 h.

cathepsin B expression was also carried out in the absence and presence of antipain hydrochloride inhibitor. As shown in Figure 6B and Figure S5B (Supporting Information), NIH-3T3 cell treated with free DOX could lead to obvious cytotoxicity, which was similar to the results observed in other cells with free DOX incubation. However, compared with free DOX, there was much lower cytotoxicity observed in the controlled cells when the different concentrations of enzyme-responsive DOX-loaded CPP-QDs@$mSiO_2$ nanoconjugates were employed, further indicating the different cell uptake mechanism for free DOX and DOX-loaded CPP-QDs@$mSiO_2$ as indicated in other cells previously. The observed cytotoxicity was also found more limited than those enzyme expressed cells treated with the same concentrations of DOX-loaded CPP-QDs@$mSiO_2$, and similar low cytotoxicity was further found when the drug nanoconjugate-incubated NIH-3T3 cells were treated with cathepsin B inhibitor, clearly suggesting that lack of specific cathepsin B expression in this cell line environment would not activate the significant nucleus-targeted DOX release from CPP-QDs@$mSiO_2$ surface and thus lead to the limited drug activity against NIH-3T3. These results unequivocally suggested that the CPP-QDs@$mSiO_2$ could be used as efficient activatable delivery cargoes to sensitively respond to the specific tumor environmental enzymes and significantly improve the antitumor activities by selectively directing the chemotherapeutic agents into targeted cell nucleus, especially for those cells with potent drug-resistant properties.

3. Conclusions

We have presented a set of novel and personalized nanocarriers for the controlled nucleus-targeted antitumor drug delivery and real-time imaging of intracellular drug trafficking by integrating an enzyme activatable CPP sequence with mesoporous silica-coated QDs nanoparticles. The systematic cytotoxicity and imaging studies confirmed that the drug-loaded QDs@$mSiO_2$ nanoparticles could selectively control the localized drug delivery into the nucleus of targeted tumor cells with high cathepsin B expression and thus elicit significant tumor cytotoxicity with minimum side effects, especially to cells with drug-resistant properties. Moreover, the enzyme-responsive nuclear-targeted drug delivery nanoconjugates could also demonstrate promising functions to perform real-time imaging of the process of targeting and intracellular delivery through the fluorescence of QDs@$mSiO_2$. Such specific and personalized enzyme-responsive nuclear-targeted CPP-QDs@$mSiO_2$ nanoparticles may provide a useful strategy to achieve selective nuclear-targeted delivery of therapeutic reagents, and it may also facilitate the rational design of new transport cargo for enhanced drug activity against tumor cells including those can easily generate drug resistance.

4. Experimental Section

Materials: All Fmoc-protected amino acids were purchased from Bachem or GLchem. Other chemical reagents used were either bought from Aldrich or Fluka. Protease enzyme cathepsin B and its inhibitor, antipain hydrochloride, were purchased from Sigma–Aldrich. The Mal-PEG_2-NHS linker was purchased from Quanta Biodesign. All commercially available reagents discussed were used without further purification.

Instruments: Mass spectra were measured on a Thermo LCQ Deca XP MAX instrument for ESI measurements. HPLC analysis was performed on a reverse-phase column with a Shimadzu HPLC system. UV absorption spectra were recorded on a Beckman coulter DU800 spectrometer. Fluorescence emission spectra were performed on a Varian Cary eclipse fluorescence spectrophotometer. The SEM and TEM images were collected on transmission electron microscope (JEOL JEM-1400) and scanning electron microscope (JEOL JSM-7600F).

Synthesis of Quantum Dots (QDs) Nanoparticles: The synthesis of QDs nanoclusters was carried out described previously.[16] Briefly, 1.401 g (3.35 mmol) of $Cd(ClO_4)_2{\cdot}6H_2O$ was dissolved in 180 mL of deionized water, followed by addition of 0.11 mL (1.53 mmol) of mercaptoacetic acid (TGA). The pH of the reaction mixture was then adjusted to 11.2 using 5 M NaOH solution. Then, H_2Te gas, carried by a flow of N_2, was introduced into the reaction mixture while maintaining vigorous stirring. Upon the reaction for ≈20 min, the resultant orange solution was subjected to reflux to afford the final product of QDs nanoparticles.

Synthesis of Mesoporous Silica-Coated QDs (QDs@$mSiO_2$): The silica-coated QDs nanoparticles (QDs@SiO_2) were prepared on the basis of a reverse micro-emulsion method.[17] Typically, a 50 µL of prepared QDs aqueous solution and 250 µL of aqueous ammonia (25 wt%) were introduced into a liquid system containing 10 mL of cyclohexane, 2 mL of *n*-hexanol, and 2 mL of tritonX-100. Subsequently, 50 µL tetraethyl orthosilicate (TEOS) and 10 µL (3-aminopropyl) triethoxysilane (APS) were introduced under vigorous stirring. The reaction vessel was then sealed and kept in the dark at room temperature for 2 d. Finally, acetone was used to terminate the reaction and the resultant precipitate was washed in sequence with butanol, isopropyl alcohol, ethanol, and water to produce an aqueous suspension of the composite silica-coated QDs nanoparticles with amino groups on the surface, which were used for further characterization.

The mesoporous silica-coated QDs (QDs@$mSiO_2$) were synthesized through a NaOH-based etching method.[17] Briefly, 1 mL of 0.1 g mL^{-1} aqueous sodium hydroxide (NaOH) was added to a 4-mL solution of the prepared silica-coated QDs (2 mg mL^{-1}) and the mixture was stirred at room temperature for 1 h. Upon etching of silica, which coated on QDs particles surface, the clear solutions became opaque. Then, the QDs@$mSiO_2$ nanoparticles were washed with water. After repeated washing and centrifugation, the prepared colloidal spheres were generated, which were finally dispersed in polar solvents such as deionized water or ethanol for further applications.

Synthesis of Enzyme-Responsive Cell-Penetrating Peptides (CPPs): The enzyme-responsive CPPs (CRRRQRRKKR-PGFK-EEEEEE) were prepared by solid-phase peptide synthesis (SPPS). The final CPPs product was purified by HPLC and further characterized by ESI-MS. ESI-MS: m/z 2644.94 (calcd); 661.03 m/4z, 1320.61 m/2z (found).

Conjugation of the Enzyme-Responsive CPPs with QDs@$mSiO_2$: The as-prepared QDs@$mSiO_2$ (5 mg) were dissolved in dimethylformamide (DMF, 100 µL) and then 100 µL of Mal-dPEG_2-NHS ester in DMF (20×10^{-3} M) was added along with triethylamine (TEA, 2 µL). The reaction mixture was stirred in the dark for 20 h. Finally, the Mal-PEG-functionalized nanoparticles were collected and washed with DMF three times. To the suspension of Mal-PEG-modified nanoparticles (5 mg) in DMF (100 µL), the enzyme-responsive cell-penetrating CPP (5×10^{-3} M, 300 µL in DMF) prepared by solid-phase synthesis and TEA (2 µL) was added and the reaction was continued for 24 h under the same conditions. After collection of the CPP-conjugated QDs@$mSiO_2$ nanoparticles by centrifugation, the final product was washed with DMF/EtOH (v:v = 1:5) three times, followed by washing with phosphate-buffered saline solution (PBS, 0.1 M, pH 7.2) for another three times. The final product was suspended in PBS for the subsequent biological tests. The similar nucleus-targeted TAT-QDs@$mSiO_2$ nanoparticles were also synthesized by using this method, which were used as controls.

Living Cell Assay: The cell lines including A549, NIH-3T3, antitumor drug nonresistant A2780, and resistant A2780/Adr were purchased from the American-type culture collection (ATCC). All the cells were cultured regularly in growth medium consisting of DMEM supplemented with 10% FBS (fetal bovine serum, Invitrogen, Burlington, Canada), at 37 °C in a humidified atmosphere with a 5% CO_2 concentration, using a 35-mm diameter plastic bottom dish (ibidi GmbH, Germany). The cells were routinely harvested by treatment with a trypsin-ethylenediaminetetraacetic acid (EDTA) solution (0.25%) (Invitrogen, Burlington, Canada).

MTT Cell Viability Assay: The standard MTT assay was used to measure the cytotoxicity of the enzyme-responsive CPP-QDs@mSiO_2 nanoparticles and the cell viability of antitumor drug DOX-loaded CPP-QDs@mSiO_2 nanoparticles. Briefly, the cells were plated at a density of ≈10 000 cells per well, in a 96-well flat-bottomed microplate (Corning Inc, New York, USA) with 100 µL of cells suspension per well. The CPP-QDs@mSiO_2 nanoparticles were tested at concentrations ranging from 0 to 1000 µg mL^{-1}. The CPP-QDs@mSiO_2 nanoparticles were incubated with the cells for 24 h. Then, the cells were incubated with MTT reagent at 37 °C for 3 h prior to the removal of the DMEM. Upon cell lysis, the intracellular formazan product was dissolved using 100 µL DMSO and then quantified by Infinite F200 (Tecan Inc, Switzerland) at a wavelength of 490 nm. The relative cell growth (%) was calculated by (test/control) × 100, where the control contained only cell and culture medium.

Live Cell Imaging by Confocal Laser Scanning Microscopy (CLSM): The cells were seeded in a CLSM culture dish with a cell confluence of 50%–60% and the cell count for each culture dish (3.5 cm) was 5×10^5 cells/dish. The CPP-QDs@mSiO_2 nanoparticles and DOX-loaded CPP-QDs@mSiO_2 were dispersed into cell culture medium at a concentration of 50 µg mL^{-1} and then added to dish for cell incubation under different time durations (4 and 24 h). Then, the cells were washed three times with PBS and incubated with 100 µL of 4,6-diamidino-2-phenylindole (DAPI) (50 µg mL^{-1}) for 30 min to stain the nuclei. The cells were then washed three times with PBS to remove excessive DAPI. Finally, 1 mL of PBS was added and the cells were visualized using CLSM (LSM 510, Zeiss, Germany). The fluorescence images were taken using a 63× oil-immersion objective lens with DAPI, and QDs@mSiO_2, and DOX excited at wavelength of 405 (DAPI), 405 (QDs@mSiO_2), and 488 nm (DOX). The cellular endo/lysosome colocalization measurement was conducted by using the green fluorescent protein (GFP) fused lysosome-associated membrane protein 1 (LAMP1, one commonly applied lysosome tracker, Invitrogen, Excitation: 488 nm). The fluorescent signals were collected on the basis of the emission filter sets of 450/25, 550/30, 530/30, and 630/30 nm for DAPI, LAMP1, CPP-QDs@mSiO_2, and free DOX, respectively.

DOX Loading and Release from the Enzyme-Responsive CPP-QDs@mSiO$_2$: 5 mg of the CPP-QDs@mSiO_2 were mixed with 10 mL DOX (0.5 mg mL^{-1}) solution in PBS solutions. After over night reaction, the DOX-loaded CPP-QDs@mSiO_2 nanoparticles were washed by PBS and then collected by centrifugation. To evaluate the DOX-loading capacity, the loaded DOX content was determined by UV–vis measurements at the wavelength of 480 nm upon removal of the background of CPP-QDs@mSiO_2.[20] To test the DOX release efficiency, the enzyme-responsive DOX-loaded nanoparticles were used to react with cathepsin B protease (50×10^{-9} M) under different pH (5.0 or 7.4) in the presence or absence of antipain hydrochloride inhibitor (50×10^{-6} M) to control release the DOX from the nanoparticles. Upon the enzyme treatment at various time durations (e.g., 2, 4, 6, 8, and 12 h, respectively), the supernatant solution was collected to determine the content of released DOX from the nanoparticles by measurements the absorbance or fluorescence of DOX drug.

Supporting Information

Supporting Information is available from the Wiley Online Library or from the author.

Acknowledgements

This work was supported by Start-Up Grant (SUG), PSF (SERC1121202008), MOE, Tier 1 (RG 64/10), COS research collaboration award in Nanyang Technological University, Singapore.

Received: November 5, 2013
Revised: January 25, 2014
Published online: February 18, 2014

[1] A. Jemal, F. Bray, M. M. Center, J. Ferlay, E. Ward, D. Forman, *CA: A Cancer J. Clin.* **2011**, *61*, 69.
[2] M. M. Gottesman, T. Fojo, S. E. Bates, *Nat. Rev. Cancer* **2002**, *2*, 48.
[3] a) M. E. Davis, Z. G. Chen, D. M. Shin, *Nat. Rev. Drug Discovery* **2008**, *7*, 771; b) D. Peer, J. M. Karp, S. Hong, O. C. FaroKhzad, R. Margalit, R. Langer, *Nat. Nanotechnol.* **2007**, *2*, 751; c) T. M. Allen, P. R. Cullis, *Science* **2004**, *303*, 1818; d) K. Cho, X. Wang, S. M. Nie, Z. G. Chen, D. M. Shin, *Clin. Cancer Res.* **2008**, *14*, 1310; e) L. Brannon-Peppas, J. O. Blanchette, *Adv. Drug Delivery Rev.* **2012**, *64*, 206; f) W. B. Cai, X. Y. Chen, *Small* **2007**, *3*, 1840; g) X. X. He, K. M. Wang, Z. Cheng, *Wiley Interdiscip. Rev. Nanomed. Nanobiotechnol.* **2010**, *2*, 349; h) X. Q. Chi, D. T. Huang, Z. H. Zhao, Z. J. Zhou, Z. Y. Yin, J. H. Gao, *Biomaterials* **2012**, *33*, 189; i) K. Yang, L. Z. Feng, X. Z. Shi, Z. Liu, *Chem. Soc. Rev.* **2013**, *42*, 530; j) D. J. Irvine, *Nat. Mater.* **2011**, *10*, 342; k) R. A. Petros, J. M. DeSimone, *Nat. Rev. Drug Discovery* **2010**, *9*, 615; l) C. Xu, S. Sun, *Adv. Drug Delivery Rev.* **2013**, *65*, 732; m) K. Saha, S. S. Agasti, C. kim, X. N. Li, V. M. Rotello, *Chem. Rev.* **2012**, *112*, 2739; n) L. Cheng, C. Wang, Z. Liu, *Nanoscale* **2013**, *5*, 23.
[4] T. G. Iversena, T. Skotlanda, K. Sandvig, *Nanoday* **2011**, *6*, 176.
[5] a) E. Koren, V. P. Torchilin, *Trends Mol. Med.* **2012**, *18*, 385; b) S. B. Fonseca, M. P. Pereira, S. O. Kelley, *Adv. Drug Delivery Rev.* **2009**, *61*, 953.
[6] a) L. A. Austin, B. Kang, C. W. Yen, M. A. El-Sayed, *J. Am. Chem. Soc.* **2011**, *133*, 17594; b) Y. L. Wang, J. J. Chen, J. Irudayaraj, *ACS Nano* **2011**, *5*, 9718; c) J. H. Liu, Y. X. Zhao, Q. Q. Guo, Z. Wang, H. Y. Wang, Y. X. Yang, Y. Z. Huang, *Biomaterials* **2012**, *33*, 6155; d) E. Oh, J. B. Delehanty, K. E. Sapsford, K. Susumu, R. Goswami, J. B. Blanco-Canosa, P. E. Dawson, J. Granek, M. Shoff, Q. Zhang, P. L. Goering, A. Huston, I. L. Medintz, *ACS Nano* **2011**, *5*, 6434; e) Z. Krpetić, S. Saleemi, I. A. Prior, V. Sée, R. Qureshi, M. Brust, *ACS Nano* **2011**, *5*, 5195; f) H. Park, H. Tsutsumi, H. Mihara, *Biomaterials* **2013**, *34*, 4872.
[7] a) I. Martín, M. Teixidó, E. Giralt, *Curr. Pharm. Des.* **2013**, *19*, 2924; b) B. R. Liu, Y. W. Huang, J. G. Winiarz, H. J. Chiang, H. J. Lee, *Biomaterials* **2011**, *32*, 3520; c) M. Zhou, I. Ghosh, *Biopolymers* **2007**, *88*, 325; d) X. Q. Chi, D. T. Huang, Z. H. Zhao, Z. J. Zhou, Z. Y. Yin, J. H. Gao, *Biomaterials* **2012**, *33*, 189.
[8] a) L. M. Pan, Q. J. He, J. N. Liu, Y. Chen, M. Ma, L. L. Zhang, J. L. Shi, *J. Am. Chem. Soc.* **2012**, *134*, 5722; b) Y. P. Chen, C. T. Chen, Y. Hung, C. M. Chou, T. P. Liu, M. R. Liang, C. T. Chen, C. Y. Mou, *J. Am. Chem. Soc.* **2013**, *135*, 1516.
[9] J. N. Liu, W. B. Bu, L. M. Pan, S. J. Zhang, F. Chen, L. P. Zhou, K. L. Zhao, W. J. Peng, J. L. Shi, *Biomaterials* **2012**, *33*, 7282.
[10] a) L. Agemy, D. Friedmann-Morvinski, V. R. Kotamraju, L. Roth, K. N. Sugahara, O. M. Girard, R. F. Mattrey, I. M. Verma, E. Ruoslahti, *Proc. Natl. Acad. Sci.* **2011**, *108*, 17450; b) H. P. Song, J. Y. Yang, S. L. Lo, Y. Wang, W. M. Fan, X. S. Tang, J. M. Xue, S. Wang, *Biomaterials* **2010**, *31*, 769; c) C. A. Smith, J. de la Fuente, B. Pelaz, E. P. Furlani, M. Mullin, C. C. Berry, *Biomaterials* **2010**, *31*, 4392; d) H. W. Child, P. A. Del Pino, J. M. De La Fuente, A. S. Hursthouse, D. Stirling, M. Mullen, G. M. McPhee, C. Nixon, V. Jayawarna, C. C. Berry, *ACS Nano* **2011**, *5*, 7910.

[11] a) E. L. Jin, B. Zhang, X. R. Sun, Z. X. Zhou, X. P. Ma, Q. H. Sun, J. B. Tang, Y. Q. Shen, E. Van Kirk, W. J. Murdoch, M. Radosz, *J. Am. Chem. Soc.* **2013**, *135*, 933; b) G. Sharma, A. Modgil, B. Layek, K. Arora, C. Sun, B. Law, J. Singh, *J. Controlled Release* **2013**, *167*, 1.

[12] a) E. Koren, A. Apte, A. Jani, V. P. Torchilin, *J. Controlled Release* **2012**, *160*, 264; b) K. Kono, S. Nakashima, D. Kokuryo, I. Aoki, H. Shimomoto, S. Aoshima, K. Maruyama, E. Yuba, C. Kojima, A. Harada, Y. Ishizaka, *Biomaterials* **2011**, *32*, 1387; c) V. P. Torchilin, *Adv. Drug Delivery Rev.* **2006**, *58*, 1532; d) A. A. Kale, V. P. Torchilin, *Methods Mol. Biol.* **2010**, *605*, 213; e) H. Hatakeyama, H. Akita, H. Harashima, *Adv. Drug Delivery Rev.* **2011**, *63*, 152.

[13] a) T. Jiang, E. S. Olson, Q. T. Nguyen, M. Roy, P. A. Jennings, R. Y. Tsien, *Proc. Natl. Acad. Sci.* **2004**, *101*, 17867; b) E. S. Olson, T. Jiang, T. A. Aguilera, Q. T. Nguyen, L. G. Ellies, M. Scadeng, R. Y. Tsien, *Proc. Natl. Acad. Sci.* **2010**, *107*, 4311; c) K. Y. Lin, G. A. Kwong, A. D. Warren, D. K. Wood, S. N. Bhatia, *ACS Nano* **2013**, *7*, 9001; d) S. X. Huang, K. Shao, Y. Y. Kuang, Y. Liu, J. F. Li, S. An, Y. B. Gao, H. J. Ma, X. He, C. Jiang, *Biomaterials* **2013**, *34*, 5294; e) S. X. Huang, K. Shao, Y. Y. Kuang, Y. Liu, J. F. Li, S. An, Y. B. Gao, H. J. Ma, C. Jiang, *ACS Nano* **2013**, *7*, 2860.

[14] a) U. Resch-Genger, M. Grabolle, S. Cavaliere-Jaricot, R. Nitschke, T. Nann, *Nat. Methods* **2008**, *5*, 763; b) L. Igor, H. Medintz, T. Uyeda, E. R. Goldman, H. Mattoussi, *Nat. Mater.* **2005**, *4*, 435; c) X. Michalet, F. F. Pinaud, L. A. Bentolila, J. M. Tsay, S. Doose, J. J. Li, G. Sundaresan, A. M. Wu, S. S. Gambhir, S. Weiss, *Science.* **2005**, *307*, 538; d) A. M. Smith, H. W. Duan, A. M. Mohs, S. M. Nie, *Adv. Drug Delivery Rev.* **2008**, *60*, 1226; e) Y. Xing, J. H. Rao, *Cancer Biomark* **2008**, *4*, 307; f) P. Zrazhevskiy, M. Sena, X. H. Gao, *Chem. Soc. Rev.* **2010**, *39*, 4326; g) C. E. Probst, P. Zrazhevskiy, V. Bagalkot, X. H. Gao, *Adv. Drug Delivery Rev.* **2013**, *65*, 703; h) V. Biju, T. Itoh, M. Ishikawa, *Chem. Soc. Rev.* **2010**, *39*, 3031; i) J. H. Gao, X. Y. Chen, Z. Cheng, *Curr. Top. Med. Chem.* **2010**, *10*, 1147; j) V. Biju, S. Mundayoor, R. V. Omkumar, A. Anas, M. Ishikawa, *Biotechnol. Adv.* **2010**, *28*, 199; k) V. Biju, T. Itoh, A. Anas, A. Sujith, M. Ishikawa, *Anal. Bioanal. Chem.* **2008**, *391*, 2469.

[15] a) F. Lecaille, J. Kaleta, D. Bromme, *Chem. Rev.* **2002**, *102*, 4459; b) K. Miller, R. Erez, E. Segal, D. Shabat, R. Satchi-Fainaro, *Angew. Chem Int. Ed.* **2009**, *121*, 2993; c) S. Lee, K. Park, K. Kim, K. Choi, I. C. Kwon, *Chem. Commun.* **2008**, *28*, 4250; d) F. Gong, X. Peng, C. Luo, G. Shen, C. Zhao, L. Zou, L. Li, Y. Sang, Y. Zhao, X. Zhao, *Mol. Cancer* **2013**, *12*, 125; e) Y. M. Yang, J. X. Aw, K. Chen, F. Liu, P. Padmanabhan, Y. L. Hou, Z. Cheng, B. G. Xing, *Chem. Asian J.* **2011**, *6*, 1381.

[16] Y. H. Yang, M. Y. Gao, *Adv. Mater.* **2005**, *17*, 2354.

[17] Q. Zhang, T. R. Zhang, J. P. Ge, Y. D. Yin, *Nano Lett.* **2008**, *8*, 2867.

[18] a) U. Kubitscheck, D. Grnwald, A. Hoekstra, D. Rohleder, T. Kues, J. P. Siebrasse, R. J. Peters, *J. Cell Biol.* **2005**, *168*, 233; b) A. C. Meinema, J. K. Laba, R. A. Hapsari, R. Otten, F. A. A. Mulder, A. Kralt, G. van den Bogaart, C. P. Lusk, B. Poolman, L. M. Veenhoff, *Science* **2011**, *333*, 90.

[19] M. Vaccari, A. Argnani, W. Horn, P. Silingardi, M. Giungi, M. G. Mascolo, S. Bartoli, S. Grilli, A. Colacci, *Anticancer Res.* **1999**, *19*, 589.

[20] a) J. Kim, J. Lee, J. Lee, J. Yu, B. Kim, K. An, Y. Hwang, C. Shin, J. Park, J. Kim, T. Hyeon, *J. Am. Chem. Soc.* **2006**, *128*, 688; b) J. E. Lee, N. Lee, H. Kim, J. Kim, J. Kim, S. H. Choi, J. H. Kim, T. Kim, I. C. Song, S. P. Park, W. K. Moon, T. Hyeon, *J. Am. Chem. Soc.* **2010**, *132*, 552; c) L. Zhu, T. Ikoma, N. Hanagata, S. Kaskel, *Small* **2010**, *6*, 471; d) M. K. Yu, Y. Y. Jeong, J. Park, S. Park, J. W. Kim, J. J. Min, K. Kim, S. Jon, *Angew. Chem Int. Ed.* **2008**, *47*, 5362; e) Y. M. Yang, B. Velnurugan, X. G. Liu, B. G. Xing, *Small* **2013**, *9*, 2937.

[21] a) K. M. Tewey, T. C. Rowe, L. Yang, B. D. Halligan, L. F. Liu, *Science* **1984**, *226*, 466; b) R. W. Johnstone, A. A. Ruefli, S. W. Lowe, *Cell* **2002**, *108*, 153.

